Microscopic studies of polycrystalline nanoparticle growth in free space

Microscopic studies of polycrystalline nanoparticle growth in free space

A. Mohan (1), M. Kaiser (2), M. A. Verheijen (2) (3), R.E.I. Schropp (3) and J.K. Rath (1)

1. Utrecht University, Faculty of Science, Debye Institute for Nanomaterials Science-Physics of Devices, High Tech Campus 21, 5656 AE Eindhoven, the Netherlands
2. Philips Innovation Services, Materials Analysis, High Tech Campus 11, 5656 AE Eindhoven, the Netherlands
3. Eindhoven University of Technology (TU/e), Department of Applied Physics, Plasma & Materials Processing, P.O. Box 513, 5600 MB Eindhoven, the Netherlands

ABSTRACT: We have extensively studied by multiple microscopic techniques the growth and crystallization of silicon nanoparticles in pulsed SiH_4/Ar plasmas. We observe that the crystallinity of the particles can be tuned from amorphous to crystalline by altering the plasma ON time, t_{ON}. Three phases can be identified as a function of t_{ON}. Microscopic studies reveal that, in the initial gas phase (phase I) single particles of polycrystalline nature are formed which according to our hypothesis grow out of a single nucleus. The individual crystallites of the polycrystalline particles become bigger crystalline regions which marks the onset of cauliflower shaped particles (phase II). At longer t_{ON} (phase III) distinct cauliflower particles are formed by the growth of these crystalline regions by local epitaxy.

INTRODUCTION

The increasing interest in silicon nanoparticles (NPs) is because of new opportunities to use them for widespread potential applications in nano-electronic devices [1], light emitting diodes [2], photovoltaic devices [3] and biological applications [4]. The size and size distribution have a strong influence on the optical and electrical properties of nanostructured materials and thus precise control of the particle size is a prerequisite to exploit their size dependent optoelectronic properties. Pulsed radio frequency (RF) discharge is known to be very effective in suppressing powder concentration in the discharge volume [5]. Fine tuning the parameter space with this technique, pulsing of a silane plasma made by RF plasma enhanced chemical vapor deposition (RF PECVD) has shown to help grow quantum-sized nanocrystalline silicon (nc-Si) particles with a narrow size distribution [6]. Precise size control of NPs can be obtained by varying the gas residence time in the discharge region or by pulsing the RF power ON (t_{ON}) and OFF times (t_{OFF}). Particle growth can be controlled by varying the plasma ON time. As a consequence the photoluminescence (PL) spectra can be tuned, by changing the t_{ON} [7]. Plasma OFF time is critical in refreshing the source gases in the discharge area and t_{OFF} longer than the gas residence time is found to be favorable for obtaining quantum sized particles [8].

One of the first experimental evidences of a multistep growth process of NPs in a silane-argon low pressure discharge was given by A. Bouchoule and L. Boufendi [9], who interpreted their results by invoking a process that involves nucleation and agglomeration, followed by silicon deposition on growing particles. An analytical model of the particle growth is considered and shown to be a three step phenomenon [10]. According to this model, the first generation of supersmall (2 nm) particles grow as a

chain of negative-ion molecular reactions, stimulated by vibrational excitation. As the cluster size increases, their probability of reaction with vibrationally excited molecules decreases, limiting the size of first generation particles. The negative particles and the neutral particles which have acquired a negative charge are trapped in the discharge. During the agglomeration phase the NPs acquire a negative charge and the Coulomb repulsion becomes stronger. After a certain threshold value, the agglomeration phase stops and the NPs continue to grow by radical deposition on their surface [9]. These trapped particles coagulate and a critical phenomenon of α to γ` transition takes place when the particle size increases and their concentration in the plasma decreases dramatically, altering the plasma parameters [11]. This theoretical approach is in good agreement with effects observed in experiments. In this paper we show that the nanoparticles *do not always grow according to the above mentioned agglomeration mechanism*. Experiments done in ETP (expanding thermal plasma) also support our hypothesis that particle formation in their system (and possibly in the systems where particle formation is strongly governed by drift and diffusion in finite growth regime) does not follow the commonly believed nucleation, agglomeration, coagulation sequence [12].

For long plasma durations (> 30 s), which is equivalent to a continuous plasma, occurrence of several well-defined particle sizes, corresponding to successive (in time) particle generations has been observed. Transmission electron microscopy (TEM) studies of Si NPs grown/formed in various plasma processes in capacitively coupled discharges show cauliflower morphology with smaller crystalline subsystems [13] [14]. The luminescence decay time of cauliflower shaped Si NPs produced in a cluster source by magnetron sputtering has been shown to be enhanced by a thousand times by the use of vacuum grease [15]. Although the mechanism of formation of these structures is not fully understood, the commonality between them is that they are composed of smaller crystalline subsystems. The aim of this paper is to study the NPs growth as a function of time in a silane plasma and propose a mechanism that ultimately leads to the observed cauliflower-structured particles. In the following sections of our paper, we report our observations in the formation and crystallization of the nanoparticles at different t_{ON} times in the gas phase by HRTEM studies.

EXPERIMENTAL

The NPs described in this paper are grown in a dedicated plasma reactor, more details of which can be found elsewhere [14] [16]. The source gases of SiH_4 and Ar are fed through the bottom showerhead electrode and are dissociated by the applied oscillating very high frequency (VHF) electric field of 60 MHz. The NPs formed in the gas phase are collected at a Corning glass substrate mounted at the top of the reactor, behind the perforated ground electrode, thanks to thermophoretic effect and the drag due to gas pumping which aids in collection of particles upstream. The radius of the electrode is 10 cm and the height (distance between the grounded electrode and the powered electrode is 1 cm). The total radius of the reactor is 16 cm.

For the particles mentioned in this paper, a SiH_4:Ar flow ratio of 4 sccm:50 sccm was used for the particle synthesis at a pressure of 0.8 mbar. A forward VHF power of 150 W was applied to the showerhead electrode, and the substrate stage was unheated. The applied power was pulsed, and a range of plasma ON times (t_{ON} = 50 ms to 60 s) was applied to study the time evolution of particle sizes

and their crystallinity. For each plasma ON time (t_{ON}) the discharge was sustained multiple times for a total duration of 45 minutes. The plasma OFF time (t_{OFF}) was kept constant at 2 s (which is longer than the residence time of gases in the reactor) for all t_{ON}. Structural characterization of deposited particles has been done with a Tecnai 10 and a JEOL ARM 200 Transmission electron microscope operated at 200 kV. This accelerating voltage – together with the beam doses used – is sufficient to avoid defect generation in bulk silicon. As nanoparticles may be more sensitive to electron beam irradiation, care was taken to minimize the dose used for imaging. Comparison of images taken from the same area at various stages of the TEM study did not show any tendency to particle coalescence. Fast Fourier Transform (FFT) analysis of High resolution TEM (HRTEM) images was used to detect local crystal orientations within the particles studied. Analysis of the periodicities in each of the FFT patterns yielded lattice constants that were within 1% of the 0.5428 nm lattice parameter of cubic silicon. The crystalline ratio was calculated [17] from Raman spectra obtained *ex situ* with an inVia Renishaw microscope equipped with a laser with a wavelength of 514.5 nm, a grating with 1800 lines mm^{-1} and a CCD detector to study the vibrational modes of the nanoparticles. The laser power was kept low, at 0.3 W mm^{-2} with a spot size of approximately 500 μm^2 to ensure that we do not crystallize the samples.

RESULTS

To understand the time evolution of the formation of particles and their progress into cauliflower shaped particles, the properties of the collected particles are studied as a function of t_{ON}. Optical and structural studies are performed on particles with t_{ON} from 50 ms to 6 s at a constant t_{OFF} time of 2 s which is longer than the residence time of the gases (1 s) in the reactor.

The TEM images of the NPs grown at different t_{ON} indicate there are various successive phases in the particle formation. Phase I corresponds to NPs grown with $t_{ON} \leq 0.5$ s, phase II corresponds to NPs with $0.5 \text{ s} < t_{ON} \leq 2$ s and phase III contains NPs grown with $t_{ON} > 2$ s. The size of the particles increases with increasing t_{ON}, as expected [7] [18]. From here on the term “clustered NPs” refers to unpassivated silicon nanoparticles which tend to aggregate into larger clusters facilitated, among others, by the dangling bonds on their surface [19] [20]. The term “agglomerated NPs” correspond to the coalescence or merging of polycrystalline NPs of which the single crystalline regions (domains) grow out to become NPs with larger domains.

TEM images of phase I NPs show open 3-dimensional (branched) networks of particles that have a size of a few nm, whose formation may be attributed to polymerization. It is proposed that polymerization pathway propagates via the negative ions [21]. Theoretical investigation proposes that negative ions are the precursors to large clusters which are nucleation centers for particle formation [22]. This is attributed to the longer average residence time afforded by negatively charged clusters which allows growth of large clusters to occur. Individual particles have not been observed, which may either be due to their limited contrast on the supporting carbon membrane or because they are not present at all. The crystallinity of the NPs formed in the early stages of phase I could not be determined, most likely because of oxidation during transfer from the growth reactor to the TEM set up or simply because they are inherently amorphous. For brevity we will refer to particles of phase I as ‘amorphous’. However NPs in the later stage of phase I (t_{ON} =0.5 s), did show crystallinity and detailed HRTEM of these are reported

in the following sections. NPs observed in phases II and III have a well-defined morphology and are found both as individual and clustered particles. This distinction in morphology can be understood from the difference in residence times of the particle precursors within the plasma zone. Reports from J. Costa et al [23] support this argument and it can be formulated that the initial growth of Si powder starts with the appearance of small particles due to polymerization and as the residence time increases, cross linking between the polymeric chains increases and more compact particles are formed. The first hint of the onset of cauliflower shaped particles occurs at phase II (t_{ON} of 2 s); detailed extensive HRTEM studies on these particles are reported in the following sections. While the NPs found in phase I and II predominantly have single type of particles, in phase III, i.e. for longer t_{on}, different ensembles of particles are observed. It is beyond the scope of this paper to discuss all the different ensembles of particles and we focus our attention on the dominant particles obtained in phase III, the cauliflower shaped NPs.

It is of interest to note that the crystallinity, estimated from the Raman spectra [17], of the particles depends on t_{ON}, as shown in Fig. 1. For short t_{ON} times, i.e. particles obtained in phase I (from 0.05 s to 0.25 s) only amorphous particles are produced. In our case discernable crystallinity sets in at the end of phase I (at 0.5 s) and gradually increases with t_{ON}. For particles produced at 0.25 s, although in HRTEM a few particles were found to be crystalline, the Raman signal had only the amorphous peak. At t_{ON} of 0.5 s, a small crystalline peak makes an appearance at 520 cm^{-1} against the background of a broad amorphous spectrum. From then on the crystalline fraction gradually increases with increasing t_{ON}, and saturates for longer times. A pulsed plasma with t_{ON} >10 s is indeed almost equivalent to a continuous plasma, with respect to the formed particles.

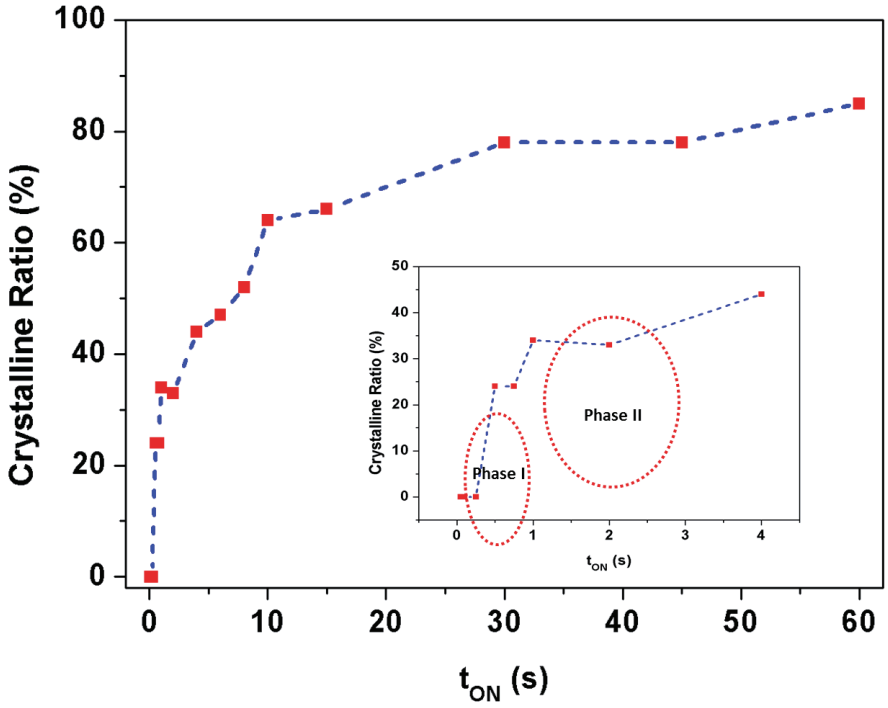

Fig. 1 : Raman crystalline ratio of the deposited NPs as a function of t_{ON}*. The inset gives the zoomed in image at the smaller values of* t_{ON}*, indicating the early phases I and II by the dotted circle.*

Various plasma process parameters such as coupled power, process pressure, gas flow, and source gas ratios (SiH_4:H_2) and inter-electrode distance play crucial roles in determining the size and crystallinity of the synthesized Si nanoparticles (NPs). We have performed an extensive study on the synthesis of silicon nanoparticles in the gas phase in a capacitively coupled VHF discharge as a function of crystalline ratio by changing the above parameters and highlighted the interdependence of crystalline ratio and residence time [24]. In this reference we changed the residence time both by changing the pressure and inter-electrode distance. The crystalline ratio is determined by surface effects driving local epitaxial growth.

HRTEM of particles produced at t_{ON} = 0.5 s (Phase I)

As stated above, the first crystallinity could be detected by Raman spectroscopy for particles made with t_{ON} = 0.5 s. Subsequent HRTEM studies of free-standing particles was performed to avoid overlap between different particles. Fig. 2 (a) and (b) give an overview of the NPs detected in the images and we identified particles in these regions. Detailed HRTEM studies (Fig 2 (c) and (d)) show that these particles are polycrystalline. The yellow arrow in Fig. 2 (c) indicates the amorphous shell around the particles. Crystalline regions within a seemingly amorphous matrix (region marked in red) can be recognized, as shown in Fig. 2 (c). The absence of crystallinity in this matrix can have two causes: either the matrix is indeed amorphous or, alternatively, the matrix consists of (nano)crystals of which the majority is not aligned to any main crystallographic axis that would allow for lattice fringe imaging. In order to investigate further, we acquired HRTEM for a series of sample orientations w.r.t. the electron beam.

The HRTEM image of the same single particle imaged at a sample tilt angle of $\alpha = 5^\circ$ is shown in Fig. 2 (d). This image confirms the second hypothesis discussed above: the particle contains crystalline regions with different orientations which cannot be seen in a single HRTEM image. Fringes are only visible when the electron beam is aligned to the crystallographic planes. In Fig. 2 (c), the region marked in red seems to be amorphous. However for other orientations of the particle w.r.t. the electron beam, this region appears to be crystalline (Fig. 2 (d)). It should be mentioned that, although different grains appear at different positions within the NP, it cannot be excluded that the particle does contain some amorphous sub-volumes. This is because of the fact that TEM is a projection technique. Comparison of FFT patterns of selected regions within the particle studied did not yield any basic symmetry relations (such as twin-relations) between individual crystalline parts of the particle, suggesting a polycrystalline nature of randomly oriented domains. A part of the particle (region marked in white) in Fig 2 (c) is overlapping with yet another particle in the projection. This area was excluded from FFT studies. On the other hand, the evidence presented here does not exclude that the different crystalline areas are correlated by a more complex system of planar defects that did not show up in the studies we performed.

Very limited papers have reported polycrystalline Si particles formation in the gas phase. Two kinds of crystalline structures (single domain and two domains) have been produced by pulsed plasma in the gas phase [25]. While most clusters (> 99%) have single domain, a very small fraction of particles have two

domains unlike our case, where a majority of NPs has more than 2 domains. Si nanoclusters produced in magnetron sputtering inert gas condensation cluster beam source also shows polycrystalline silicon structure [26].

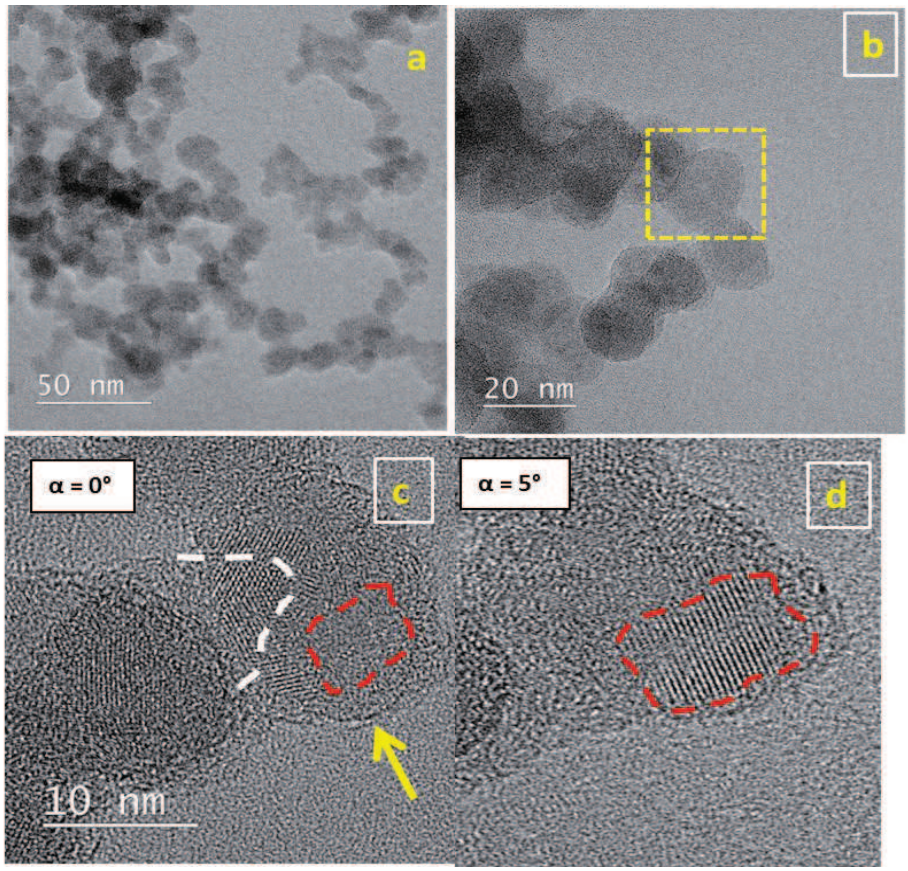

Fig 2 : (a) Overview of clustered NPs (b) Inset indicates our selected region of single NP studied at different tilt angles α (0˚ and 5˚) w.r.t. the incoming electron beam as shown in (c) and (d) respectively The region marked in red indicates amorphous nature (in Fig 2(c)), however at a different orientation, the same region is found to have crystallites (in Fig 2(d))

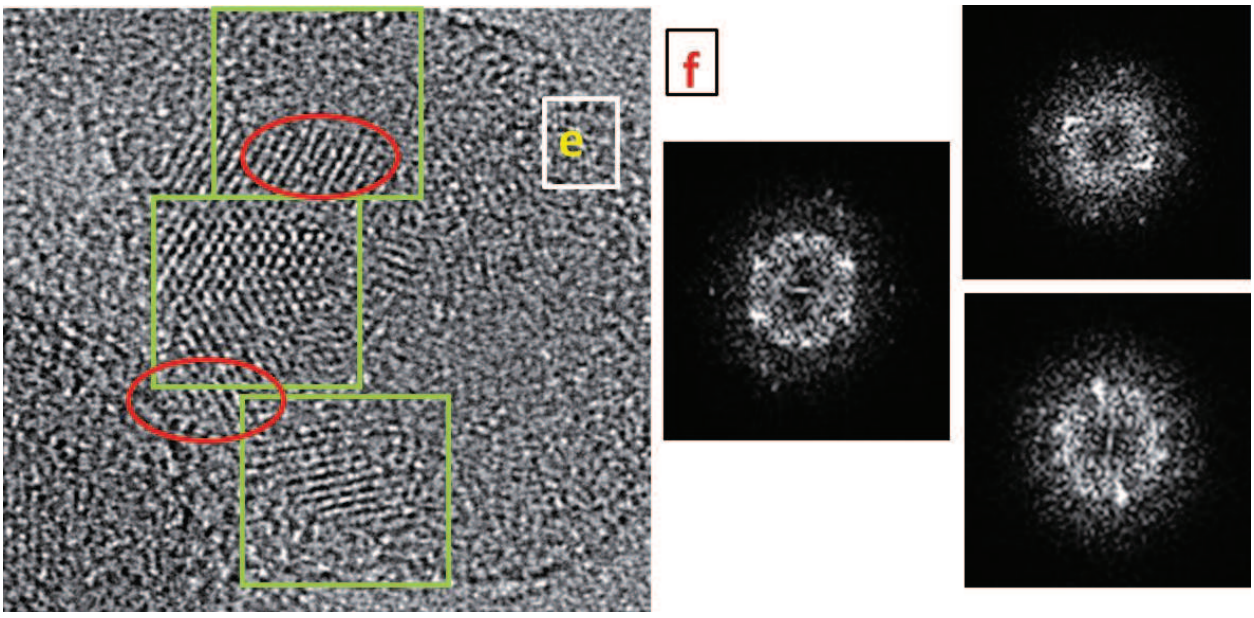

Fig. 2(e) 3 selected areas indicated by the squared boxes obtained from the HRTEM image of Fig. 2(c). The center FFT pattern is a superposition of 2 FFT patterns, originating from the 2 encircled areas. The corresponding FFT patterns from the boxed areas are displayed in (f) thus giving an indication that these areas could represent 3 individual crystals.

FFT patterns of NPs shown in Fig. 2 (e) are given in Fig. 2 (f) and are presented here to highlight the care required to interpret this type of image. The FFT patterns corresponding to the boxed areas are displayed on the right. The center FFT pattern is a superposition of periodicities from two individual crystals that largely overlap in this projected image. In the two encircled areas, parts of the individual crystals can be discerned (the upper FFT pattern represents one of the two crystals). The FFT pattern from the lower green boxed area does not display a simple symmetry relation to those of the other crystals. Thus, this analysis suggests that these areas represent three individual crystals within the same nanoparticle. A few other particles in an adjacent region were also checked using FFT pattern comparisons, and similar results were obtained. It appears that even the small particles display a complex poly-crystalline structure which could possibly be formed by the presence of many (different) crystal defects.

Inclusions of less dense material and/or material of different compositions or voids can be detected using high angular annular dark field – scanning transmission electron microscopy (HAADF-STEM) imaging. The HAADF detector uses the electrons scattered over large angles for imaging. The HAADF detector is therefore mass sensitive, which means that higher brightness in the image corresponds to the presence of (a larger concentration of) heavier atoms and vice versa. Even though the samples are contaminated severely by the oxygen plasma etch, from the HAADF-STEM of our polycrystalline particles it was seen that neither voids nor inclusions are present inside a single particle.

HRTEM of particles produced at t_{ON} = 2 s (Phase II)

NPs produced at t_{ON} of 2 s are clusters of spherical particles, which show their poly-crystalline nature more clearly. The domain size of the single-crystalline areas within each particle is significantly larger than in phase I (Fig. 3). An example of this larger domain size is the wedge-shaped domain visible in (Fig. 3 (c)). This increase in domain size is the beginning of a transition to cauliflower shaped particles, as will be discussed below.

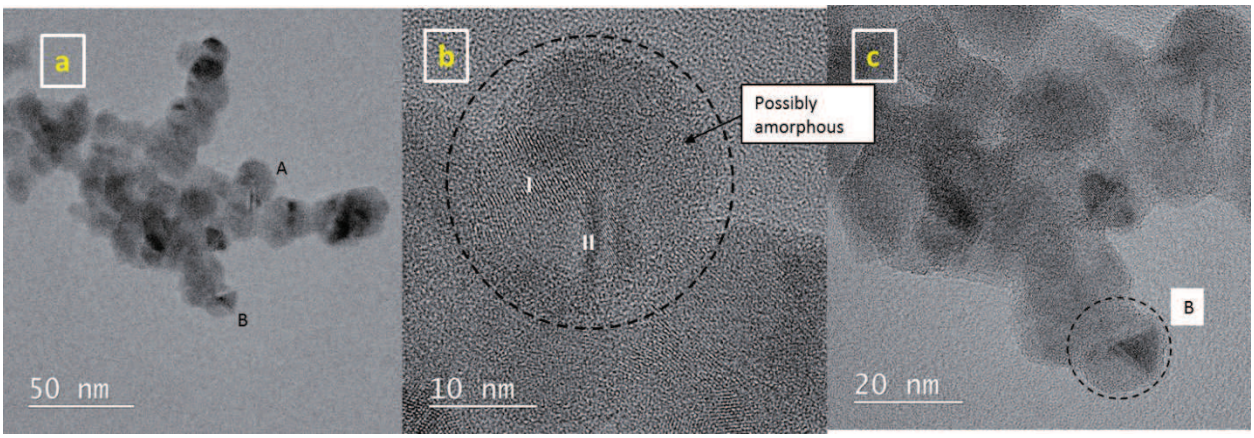

Fig. 3 : (a) Overview of NPs formed in phase II (b) and (c) HRTEM of particles in two regions A and B; the particles found at B clearly includes a wedge shaped domain.

The (at least two) crystalline regions in particle A (marked with I and II) have the same crystallographic orientation. This correlation is slightly masked by the fact that this particle has partial overlap with another particle. The vertical darker and brighter lines at the position of "II" are Moiré interference fringes [27] because of this partial overlap. The Moiré fringes have a larger spacing than the lattice fringes themselves – their interspacing strongly depending on the difference in orientation between the two grains - and thus are already visible at a magnification lower than that used for HRTEM imaging.

HRTEM of particles produced at t_{on} = 4 s (Phase III)

For longer t_{ON}, the dominant particles are the cauliflower shaped ones as shown in Fig. 4 (a). From t_{ON} = 4s to 60 s in a pulsed SiH_4/Ar plasma and in continuous plasmas we observe the appearance of cauliflower-type particles. Further HRTEM studies reveal some of their interesting structural characteristics. Fig. 4 (b) and 4 (c) displays imaging data of cauliflower particles acquired in HAADF-STEM and HRTEM modes, respectively. The dark lines in between the 'branches' of the cauliflower confirm that less material (like voids) or less dense material (like SiO_x) is present here. We interpret the dark lines as being 'crevices' which extend inwards from the surface of the cauliflower. In order to interpret this structure according to agglomeration model, we would have to assume that, in this case, three individual particles have stuck together. However, it will be a large coincidence that they fit together so perfectly with straight interfaces. In addition, the cauliflower particles display a shape with a recognizable core. We thus do not interpret this cauliflower particle as being the result of 3 particles having become connected in a later stage of the growth process.

The FFT pattern in Fig. 4 (d) corresponding to the HRTEM image of Fig. 4 (c) displays the polycrystalline nature of the entire particle. In order to study the orientation relations between the different branches of the particle, selected area FFT patterns were constructed and analyzed. The right half of the particle in Fig 4 (e) seems to consist of roughly two crystalline regions (I, II). Fig 4 (f), (g) and (h) display the corresponding selected area FFT images of the areas indicated by the green boxes.

All three FFT patterns are [011] zone axis patterns. The dashed lines in the FFT patterns are guides to the eye. In all three FFT images, these lines have the same orientation, indicating the orientation of one set of {111} planes. Patterns I and II are identical, proving that areas I and II are symmetrically equivalent, implying that they will have originated from the same nucleus. The transition area I-II shows an FFT pattern characteristic of a twinned region. On both sides of this 'transition region', the crystallographic orientation is the same. The alignment of the dark and brighter stripes in the transition region to the lattice planes in the image implies that these lines are in fact diffraction contrast variations of a series of twin domains in this transition area, similar to e.g. the multiple twinned structures in [28] .On the other hand, area III, forming the left part of the cauliflower, is a polycrystalline area having orientations (not shown here) that could not simply be correlated to the orientation of areas I and II.

It is probable that the particles discussed here originate from a single nucleus. As stated above, regions I and II are crystallographically related. What can be noticed from the images is that the twin boundaries in both regions start in the center of the particle and run outwards. It is known (from e.g. silver halide crystal growth) that the direction parallel to a twin boundary can be a fast-growing crystal direction, due to the so-called re-entrant corner effect [29]. The existence of these boundaries in the primary nucleus might thus introduce fast growing "branches" on the primary crystal which are shown in Fig 5.

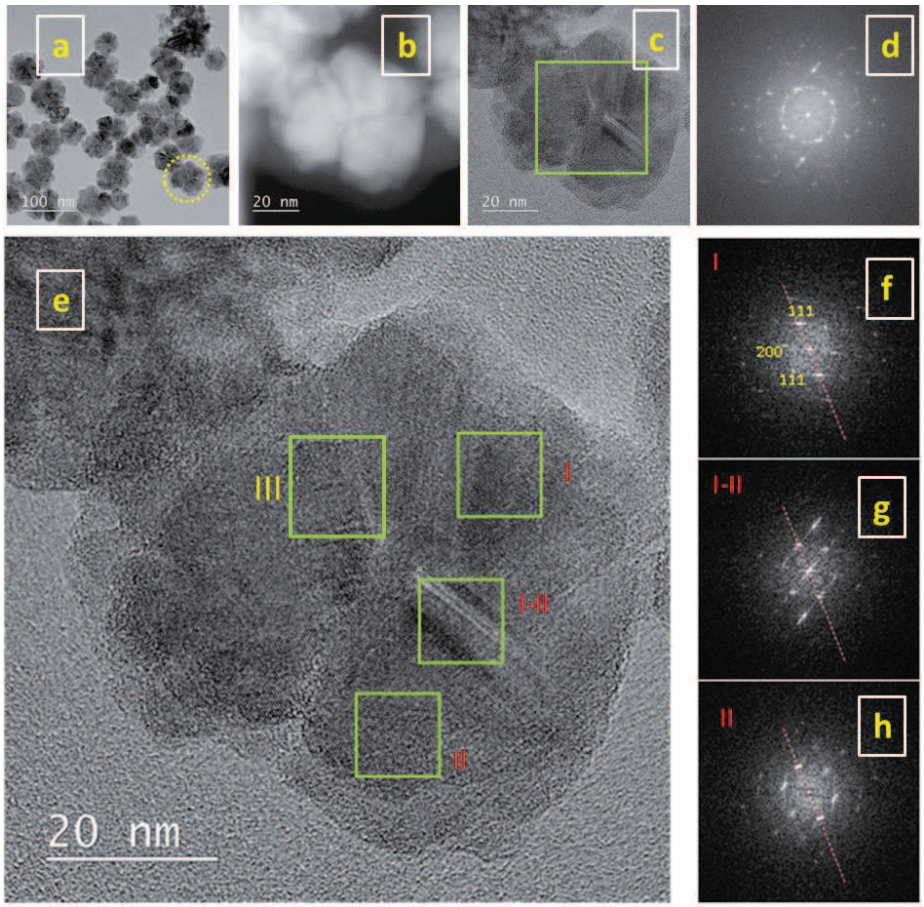

Fig. 4 : (a) Overview of cauliflower shaped nanoparticles; (b) and (c) HAADF STEM and HRTEM image of highlighted cauliflower particle respectively, (d) FFT patterns of the center of the particle covering area I, II and III, (e) HRTEM image of the highlighted particle with its 3 crystalline regions I,II and III, (f), (g) and (h) FFT pattern of regions I, I-II and II respectively

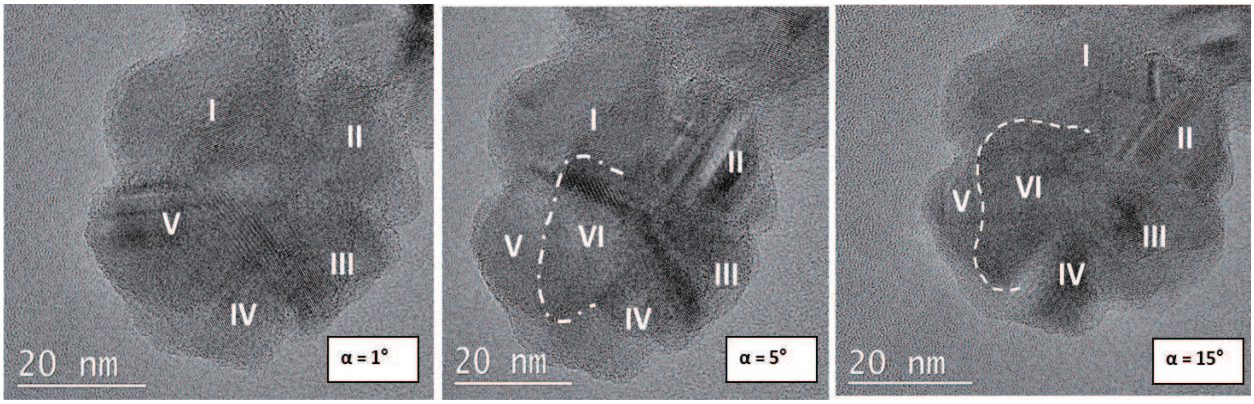

Fig. 5: HRTEM image of cauliflower particles obtained at different tilt angles. At lower tilt angles five branches are seen, at larger angles and at under-focus a 3-dimensional structure is revealed with a sixth branch (dashed line) which is not in the same plane as the other branches.

Fig. 5 displays a second type of particle that has a more compact morphology. HRTEM images were collected at sample tilts from 1° to 15°in steps of 2.5° as indicated in Fig. 5. Although only images of tilting series obtained for one sample are shown here, these studies were performed on four different particles and the same trend was observed for all series. At low tilt angles it appears as if this particle has only four branches. Upon closer inspection five branches can be discerned and after further tilting (at least) six branches were revealed. Upon tilting and adding some defocus showed a 3-D structure and revealed that these six branches are not present in the same plane. Especially the one discovered for α = 15° (dashed line) appears to be pointing out of the plane in which the other branches are present. Such a 3-D structure may severely hamper crystallinity studies as branches are overlapping in the projected images for most of the tilt range available to orient the particle w.r.t. the electron beam. FFT-studies of the non-overlapping parts revealed that not all branches have a simple (i.e. identical or single-twinned) crystallographic relation to each other. Therefore it can neither be confirmed nor excluded that this particle originated from one nucleus.

DISCUSSION

It is known that nanoparticle heating is the mechanism behind nanoparticle crystallization [30], and this can be used to understand our observation of the increase in crystalline fraction with increase in t_{ON}, an effect that can be explained as a combination of two phenomena. First, the effect of higher electron temperature at higher t_{ON} is here related to the transient nature of the initial rise of power coupled to the plasma, mainly caused by the capacitive response of instruments. The rise time has been observed by time resolved OES signal and plasma current (oscilloscope).

Although pulsed plasma offers intriguing possibilities, it presents significant challenge for power delivery and control systems such as maintaining pulsed power regulation under changing impedance condition. These issues make active impedance matching using traditional matching network almost impossible [31]. Coherent to this observations, we observe slower power matching for particles grown in phase I. The power coupling remains suboptimal for the most part of short t_{ON} and it only exponentially reaches to its delivered power. This is an inherent limitation of the VHF power source and matching network used. Thus for a short t_{ON} a stable plasma with optimum value of coupled power is not reached unlike the plasma obtained for higher t_{ON}.

The combination of these two phenomena (suboptimal power coupling at shorter t_{ON}) and higher power leading to higher crystalline fraction of particles reinforces our observation that a higher power thus delivered at longer t_{ON}, leads to higher electron temperature which aids in particle heating resulting in a higher crystalline fraction of particles.

For particles grown in phase I due to slower power matching, the power coupling remains suboptimal for the most part of short t_{ON}. This is an inherent limitation of the VHF power source and matching network used. Thus for a short t_{ON} a stable plasma with optimum value of coupled power is not reached unlike the plasma obtained for higher t_{ON}. A higher power thus delivered at longer t_{ON}, leads to higher electron temperature which aids in particle heating resulting in a higher fraction of crystalline particles [32].

The different contributions to particle heating deduced from energy balance have shown to be predominantly from recombination processes of free electrons and ions at the particle surface which acts as the heat source for crystallization of the particle. Another contribution to particle heating comes from the recombination of dissociated hydrogen (abstraction reaction) at the surface of the particle [33]. Most particulates are expected to be charged negatively and trapped in the discharge during the entire t_{ON} time, so the longer the t_{ON}, the higher is the probability of the recombination processes (free electron and ions and abstraction reactions) at the particle surface and higher the crystallinity of the particle. This study shows that t_{ON} not only controls the particle size, but also its crystallinity.

The three phases in the growth of NPs are discussed using HRTEM images and FFT studies. The particles formed at the beginning of phase I are composed of branched networks of particles with sizes of a few nm, that can be attributed to polymerization, which as discussed above are mostly amorphous. The beginning of crystallinity sets in at the end of phase I and these particles display a polycrystalline nature. Comparison of FFT patterns of selected regions within the particle did not yield any basic symmetry relations between individual crystallites of the particle. We hypothesize that the complex polycrystalline particle could originate from a single nucleus and the gas phase species are subsequently added to this growing nucleus. When it becomes energetically more favorable for the formation of a new nucleus or crystal defect on the growing surface, another crystalline domain starts. A new nucleus is formed on the surface of the growing particle and local-epitaxial growth continues enabling the formation of multiple domains. This could be one possible explanation for observation of randomly oriented multiple nanostructures.

It is very important to note that most of the single-crystalline domains observed at t_{ON} = 4 s are bigger than the single-crystalline regions in the smaller poly-crystalline particles produced at t_{ON} = 500 ms (Fig. 2 (c) and 4 (e)). For example, in the sample produced at t_{ON} = 500 ms typical crystalline regions of 4 - 5 nm are found with exceptions of 2 or 9 nm, and in the samples produced at t_{ON} = 4 s such single crystalline regions have dimensions of typically 13 - 16 nm with exceptions of 11 and 22 nm. The late phase I particles are thought to be the precursors of the phase II particles. This means that if the cauliflowers are formed by local epitaxy from the existing polycrystalline nanostructure, a longer t_{ON} would facilitate more particle heating resulting in epitaxial growth of the domains, hence larger crystalline areas in the NP.

We do not invoke the bulk particle temperature to explain epitaxial growth. According to the proposed nc-Si growth model, epitaxy is local in nature, the whole particle need not be in thermal equilibrium. Analogy is the nc-Si growth on a substrate in a PECVD process, where once nucleation takes place, the local epitaxial growth on crystal surface takes place [34] even though the substrate (bulk film) is kept at ~200°C which is much too low for epitaxy. Hence, in our hypothesis, the surface heating leads to local epitaxy. The second point is that the radiative cooling is considered negligible compared to conductive cooling for nanoparticles. The conductive cooling depends on the back ground pressure and it is reported that at low pressures in mbar range (as in our case), particle can build up heating in time [35] due to low conduction loss (net energy gain). The slow conductive cooling at low pressures allows the particle temperature to increase as a cumulative result of successive surface heating events and heat accumulates as time progresses.

Similarly other plasma processes [36] attributes the growth of larger crystallite particles to subsequent surface growth of the particle in an epitaxial manner once a crystalline nucleus of a few nanometers diameter is formed.

Larger particles have higher cross section for various events to occur such as particle recombination. The particles gains energy from the kinetic energy of electrons and ions, from their recombination and from reactive processes like association of atoms at the particle surface. Energy loss occurs via conduction and radiation. This energy balance will determine if there is net heating. According to simulations referred to in Uwe R. Kortshagen's review article [37], even particle in the range 1 micron shows net heating (temperature higher than gas). Larger crystals have been shown to have a lower cooling rate [26]. As crystallization is a stochastic process, slower cooling provides longer times for a phase transition to take place, as the NCs stay longer at the crystallization temperature. Hence for particles in phase III the combination of slower cooling and a larger surface area - facilitating more ion-electron recombination reactions and absorption of kinetic energy of impinging ions on their surface - leads to bigger crystalline particles. For instance for a 50 nm particle in a plasma (at a pressure of 1 Pa, T_e = 3.4 eV) the average energy of the impinging ions on the surface of the particle estimated by is 7.5 eV estimated by PIC/MCC simulations [38].

For the polycrystalline growth leading to cauliflower shaped particles an alternative mechanism could be proposed. This initial complex polycrystalline could also be interpreted to originate from more than one nucleus instead of being the result of different crystalline areas correlated by a complex system of planar defects that did not show up in the studies we performed. The simultaneous growth of multiple seeds to obtain a final nano-polycrystalline structure has been shown both experimentally and with simulations [26]. Topological analysis reveals the positions of different seeds of crystallinity. In the mentioned report, for a 9 nm particle, at least 3 individual crystallites are identified that grow separately from several nuclei of random shapes. Although from the evidence provided here, the single nucleus hypothesis seems most likely, we cannot rule out that the cauliflower shaped NPs could be formed by coalescence of more than one nucleus.

At longer t_{ON}, the resultant NPs could also be formed by agglomeration of smaller particles. These smaller particles must have become more crystalline during the process, as the temperature on particle rises with increased t_{ON}. The temperature is high enough for the defects (dislocations, slip planes, twin boundaries etc) to anneal out, allowing for an alignment of the domains. It has been demonstrated that the temperatures on the surface of 10 nm particles can reach up to 1200 K [39] and this range of temperatures would suffice for subsequent growth of crystalline regions in our case to form the "branches" of the cauliflower.

The HAADF image shows polycrystalline growth from a single nucleus is one example where the classic growth model does not always apply. We cannot claim single-point branching from all the other particles. We are aware of the other possibilities such as coalescence of different "branches" of the cauliflower particles as indicated by [9] or coagulation between oppositely charged particulates which oscillate in the electric field of the plasma to form larger particles [40]. The leaves of our cauliflower nanoparticles could also have originated in similar regions of the plasma, which could have coagulated

later. Molecular dynamic simulations have found that formation of new chemical bonds during the coalescence of two particles release energy and therefore significantly increase the particle temperature [41]. Simulations have also shown that for the coalescence of 6-nm particles temperatures of 1500 K would be required [42]. As we do not have an exact estimate of the temperature of our particles or their heating rate, we cannot rule out coalescence.

From the above arguments we may state that, if the starting material already shows a complex poly-crystalline structure as a result of many crystalline defects, then the one nucleus theory for the formation of cauliflower structure is possible. If, on the other hand, very small monocrystalline particles form agglomerates, the same structure as observed here is still possible. However, the absence of any voids or less dense regions in phase I between the multiple domains strengthen our one nucleus hypothesis compared with agglomeration. Another experimental observation that strengthens our one nucleus hypothesis is the morphology of the resultant structure. HAADF images clearly indicate a center from which these branches of the cauliflower emerge out.

CONCLUSION

Three phases of particle growth have been identified as a function of $t_{ON.}$ By changing t_{ON} both the size and crystallinity of the particles can be controlled. After gas phase reactions, we obtain nano-polycrystalline structures which we hypothesize originate from one nucleus in phase I. These poly-crystalline structures act as seeds for the growth of spherical particles in phase II. Cauliflower shaped particles appear at longer t_{ON} in phase III. Some “branches” of the cauliflower are crystallographically related to each other and we propose that they are formed from polycrystalline NPs in phase I. Although agglomeration of “branches” to the cauliflower structure cannot be ruled out, due to the absence of voids, it is more likely that they originate from the single nucleus of the particle formed in phase I.

ACKNOWLEDGEMENTS

This work is part of the joint solar programme (JSP) of Hyet Solar and the Stichting voor Fundamenteel Onderzoek der Materie FOM, which is part of the Netherlands Organisation for Scientific Research (NWO). Solliance is acknowledged for funding the TEM facility.

REFERENCES

[1] K. Nishiguchi and S. Oda, "Electron transport in a single silicon quantum structure using a vertical silicon probe," *J. Appl. Phys.,* vol. 88, p. 4186, 2000.

[2] K. D. Hirschman, L. Tsybeskov, S. P. Duttagupta and P. M. Fauchet, "Silicon-based visible light-emitting devices integrated into microelectronic circuits," *Nature,* vol. 384, p. 338, 1996.

[3] G. Conibeer, M. Green, R. Corkish, Y. Cho, E. C. Cho, C. W. Jiang, T. Fangsuwannarak, E. Pink, Y. Huang, T. Puzzer, T. Trupke, B. Richards, A. Shalav and K.l. Lin, "Silicon nanostructures for third

generation photovoltaic solar cells," *Thin Solid Films,* vol. 511–512, p. 654, 2006.

[4] X. Cheng, S. B. Lowe, P. J. Reece and J. J. Gooding, "Colloidal silicon quantum dots: from preparation to the modification of self-assembled monolayers (SAMs) for bio-applications," *Chem.Soc.Rev.,* vol. 43, p. 2680, 2014.

[5] Y. Watanabe, M. Shiratani, Y. Kubo, I. Ogawa and S. Ogi, "Effects of low-frequency modulation on rf discharge chemical vapor deposition," *Appl. Phys. Lett.,* vol. 53, p. 1263, 1988.

[6] K. Nishiguchia, S. Haraa, T. Amanoa, S. Hatatania and S. Oda, "Preparation of Nanocrystalline Silicon Quantum Dots by Pulsed Plasma Processes with High Deposition Rates," *MRS Proceedings ,* vol. 571, 1999.

[7] T. Nguyen-Tran, P. R. i Cabarrocas and G. Patriarche, "Study of radial growth rate and size control of silicon nanocrystals in square-wave-modulated silane plasmas," *Appl. Phys. Lett.,* vol. 91, p. 111501, 2007.

[8] A. Mohan, I. Poulios, R.E.I. Schropp and J.K. Rath, "Size control of gas phase grown silicon nanoparticles by varying the plasma OFF time in silane pulsed plasma," *MRS Proceedings,* vol. 1803, 2015.

[9] A. Bouchoule and L. Boufendi, "Particulate formation and dusty plasma behaviour in argon-silane RF discharge," *Plasma Sources Sci. Technol.,* vol. 2, p. 204, 1993.

[10] A. A. Fridman, L. Boufendi, T. Hbid, B. V. Potapkin and A. Bouchoule, "Dusty plasma formation: Physics and critical phenomena. Theoretical approach," *J. Appl. Phys.,* vol. 79, p. 1303, 1996.

[11] L. Boufendi, A. Bouchoule and T. Hbid, "Electrical characterization and modeling of a dust forming plasma in a radio frequency discharge," *J. Vac. Sci. Technol. A ,* vol. 14, p. 572, 1996.

[12] I. Doğan, N. J. Kramer1, R. H. J. Westermann, K. Dohnalová, A. H. M. Smets, M. A. Verheijen, T. Gregorkiewicz, and M. C. M. van de Sanden, "Ultrahigh throughput plasma processing of free standing silicon nanocrystals with lognormal size distribution," *J. Appl. Phys. ,* vol. 113, p. 134306, 2013.

[13] L. Boufendi and A. Bouchoule , "Particle nucleation and growth in a low-pressure argon-silane discharge," *Plasma Sources Sci. Technol,* vol. 3, p. 262, 1994.

[14] A. Mohan, M. M. de Jong, I. Poulios, R. E. I. Schropp and J. K. Rath, "Gas phase synthesis of two ensembles of silicon nanoparticles," *J. Phys. D: Appl. Phys. 48 ,* vol. 48, p. 375201, 2015.

[15] W. Tang, J. J. Eilers, M. A. van Huis, D. Wang, R. E. I. Schropp and M. Di Vece, "Formation and Photoluminescence of “Cauliflower” Silicon Nanoparticles," *J. Phys. Chem. C, ,* vol. 119, p. 11042,

2015.

[16] A. Mohan, R. E. I. Schropp, I. Poulios, W. J. Goedheer and J. K. Rath, "Optimizing the parameter space for increased crystallinity of silicon nanoparticles grown in the gas phase," *Phys. Status Solidi A,* vol. 1826, p. 213, 2016.

[17] E. Bustarret, M. A. Hachicha and M. Brunel, "Experimental determination of the nanocrystalline volume fraction in silicon thin films from Raman spectroscopy," *Appl. Phys. Lett. ,* vol. 52, p. 1675 , 1988.

[18] M. Shiratani, S. Maeda, K. Koga and Y. Watanabe , "Effects of Gas Temperature Gradient, Pulse Discharge Modulation, and Hydrogen Dilution on Particle Growth in Silane RF Discharges," *Jpn. J. Appl. Phys. ,* vol. 39, p. 287, 2000.

[19] P. Francis , S. Patil, C. Rajesh, S. Chakraborty, S. Mahamuni, C. V. Dharmadhikari and S. V. Ghaisas, "Electronic and optical properties of agglomerated hydrogen terminated silicon nanoparticles," *Eur. Phys. J. D,* vol. 67, p. 144, 2013.

[20] T. Hawa and M. R. Zachariah, "Coalescence kinetics of bare and hydrogen-coated silicon nanoparticles: A molecular dynamics study," *Phys. Rev. B.,* vol. 71, p. 165434, 2005.

[21] A. A. Howling, L. Sansonnens, J. L. Dorier and Ch. Hollenstein, "Time-resolved measurements of highly polymerized negative ions in radio frequency silane plasma deposition experiments," *J. Appl. Phys. ,* vol. 75, p. 1340, 1994.

[22] Seung J. Choi and Mark J. Kushner, "The role of negative ions in the formation of particles in low pressure plasmas," *J. Appl. Phys. ,* vol. 74, p. 853, 1993.

[23] J. Costa, G. Sardin, J. Campmany, J.L. AndÚjar, A. Canillas and E. Bertran, "Production of Silicon Powder by Square-Wave Modulated Rf Silane Plasma," *MRS Proceedings,* vol. 286, p. 155, 1992.

[24] A. Mohan, R. E. I. Schropp, I. Poulios, W. J. Goedheer and J. K. Rath, "Optimizing the parameter space for increased crystallinity of silicon nanoparticles grown in the gas phase," *Phys. Status Solidi A,* vol. 1826, p. 213, 2016.

[25] T. Kakeya, K. Koga, M. Shiratani, Y. Watanabe and M. Kondo, "Production of crystalline Si nano-clusters using pulsed H2 + SiH4 VHF discharges," *Thin Solid Films,* Vols. 506-507, p. 288, 2006.

[26] J. Zhao, V. Singh, P. Grammatikopoulos, C. Cassidy, K. Aranishi, M. Sowwan, K. Nordlund and F. Djurabekova, "Crystallization of silicon nanoclusters with inert gas temperature control," *Phys. Rev. B,* vol. 91, p. 035419, 2015.

[27] D. B. Williams and C. B. Carter, Transmission Electron Microscopy: A Textbook for Materials Science,

Springer, 2009.

[28] R.E. Algra, M.A. Verheijen, L.F. Feiner, W.G.G. Immink, R. Theissmann, W.J.P. van Enckevort, E. Vlieg and E.P.A.M. Bakkers, "Paired twins and {112¯} morphology in GaP nanowires," *Nano Lett,* vol. 10, p. 2349, 2010.

[29] I. Sunagawa, Crystals: Growth, Morphology & Perfection, Cambridge University Press, 2005.

[30] N. J. Kramer, R. J. Anthony, M. Mamunuru, E. S. Aydil and U.R.Kortshagen, "Plasma-induced crystallization of silicon nanoparticles," *J. Phys. D: Appl. Phys.,* vol. 47, p. 075202, 2014.

[31] D. Carter, "Optimized process performance using the Paramount/ Navigator power delivery/ Match solution," *Advanced Energy (White paper).*

[32] R. Anthony and U. Kortshagen, "Photoluminescence quantum yields of amorphous and crystalline silicon nanoparticles," *Phys. Rev. B,* vol. 80, p. 115407, 2009.

[33] H. R. Maurer and H. Kersten, "On the heating of nano- and microparticles in process plasmas," *J. Phys. D: Appl. Phys,* vol. 44, p. 174029, 2011.

[34] L. Houben, C. Scholten, M. Luysberg, O. Vetterl, F. Finger, and R. Carius, "Growth of microcrystalline nip Si solar cells: role of local epitaxy," *J. Non-Cryst. Solids,* vol. 299, p. 1189, 2002.

[35] U. R. Kortshagen, R. M. Sankaran, R. N. Pereira, S. L. Girshick, J. J. Wu and E. S. Aydil, "Nonthermal Plasma Synthesis of Nanocrystals: Fundamental Principles, Materials, and Applications," *Chem. Rev.,* vol. 116, p. 11061, 2016.

[36] L. Mangolini, E. Thimsen and U. Kortshagen, "High-Yield Plasma Synthesis of Luminescent Silicon Nanocrystals," *Nano Lett., 2005,* vol. 5, p. 655, 2005.

[37] U. R. Kortshagen, R. M. Sankaran,R. N. Pereira, S. L. Girshick, J. J. Wu and E. S. Aydil, "Nonthermal Plasma Synthesis of Nanocrystals: Fundamental Principles, Materials, and Applications," *Chem. Rev. ,* vol. 116, p. 11061, 2016.

[38] F. Galli, M. Mamunuru and U. R. Kortshagen, "The energy distribution function of ions impinging on nanoparticles in a collisional low-pressure plasma," *Plasma Sources Sci. Technol.,* vol. 21, p. 035002, 2012.

[39] M. Hirasawa, T. Orii and T. Seto, "Size-dependent crystallization of Si nanoparticles," *Appl. Phys. Lett.,* vol. 88, p. 093119, 2006.

[40] M. Shiratani, H. Kawasaki, T. Fukuzawa, T. Yoshioka, Y. Ueda, S. Singh and Y. Watanabe, "Simultaneous in situ measurements of properties of particulates in rf silane plasmas using a

polarization-sensitive laser-light-scattering method," *J. Appl. Phys.,* vol. 79, p. 104, 1996.

[41] M. R. Zachariah, M. J. Carrier, and E. Blasiten-Barojas, "Properties of Silicon Nanoparticles: A Molecular Dynamics Study," *J. Phys. Chem,* vol. 100, p. 14856, 1996.

[42] T. Hawa and M. R. Zachariah, "Coalescence kinetics of bare and hydrogen-coated silicon nanoparticles:A molecular dynamics study," *Phys Rev B,* vol. 71, p. 165434, 2005.